350 Micron Dust Emission from High Redshift Quasars

Alexandre Beelen

Radioastronomisches Institut der Universität Bonn, Auf dem Hügel 71, D-53121 Bonn, Germany

Max-Planck-Institut für Radioastronomie, Auf dem Hügel 69, D-53121 Bonn, Germany

Institut d'Astrophysique Spatiale, Bât. 121, Université de Paris XI, F-91405 Orsay, France

abeelen@astro.uni-bonn.de

and

Pierre Cox

Institut de Radioastronomie Millimetrique, St. Martin d'Heres, F-38406, France

cox@iram.fr

and

Dominic J. Benford

NASA / Goddard Space Flight Center, Code 665, Greenbelt, MD 20771

Dominic.Benford@nasa.gov

and

C. Darren Dowell

Jet Propulsion Laboratory, Mail Code 169-506, Pasadena, CA 91109

cdd@submm.caltech.edu

Attila Kovács

Caltech Institute of Technology, MS 320-47, Pasadena, CA 91125

attila@submm.caltech.edu

and

Frank Bertoldi

Radioastronomisches Institut Universität Bonn, Auf dem Hügel 71, 53121 Bonn

bertoldi@astro.uni-bonn.de

and

Alain Omont

Institut d'Astrophysique de Paris, CNRS, and Université de Paris VI, 98bis boulevard Arago, F-75014 Paris, France

omont@iap.fr

and

Chris L. Carilli

National Radio Astronomy Observatory, P.O. Box, Socorro, NM 87801, USA

ccarilli@aoc.nrao.edu

Received ______________; accepted ______________

.

ABSTRACT

We report detections of six high-redshift ($1.8 \leq z \leq 6.4$), optically luminous, radio-quiet quasars at 350 μm, using the SHARC II bolometer camera at the Caltech Submillimeter Observatory. Our observations double the number of high-redshift quasars for which 350 μm photometry is available. By combining the 350 μm measurements with observations at other submillimeter/millimeter wavelengths, for each source we have determined the temperature of the emitting dust (ranging from 40 to 60 K) and the far-infrared luminosity (0.6 to 2.2×10^{13} $L_{\odot}$). The combined mean spectral energy distribution (SED) of all high-redshift quasars with two or more rest frame far-infrared photometric measurements is best fit with a greybody with temperature of 47 ± 3 K and a dust emissivity power-law spectral index of $\beta = 1.6 \pm 0.1$. This warm dust component is a good tracer of the starburst activity of the quasar host galaxy. The ratio of the far-infrared to radio luminosities of infrared luminous, radio-quiet high-redshift quasars is consistent with that found for local star-forming galaxies.

Subject headings: infrared: QSOs, galaxies — galaxies: starburst, evolution, active quasars: individual (KUV 08086+4037, APM 08279+5255, HS 1002+4400, SDSS J1148+5251, J1409+5628, PSS 2322+1944) — infrared: ISM: continuum

1. Introduction

At high redshifts, a large fraction of the star formation occurs in very luminous ($> 10^{12}$ $L_\odot$) galaxies (Greve et al. 2005). Most of the radiation of the newly formed stars in these systems is absorbed by the dust and re-emitted at infrared (IR) wavelengths. In their rest frame, the spectral energy distribution (SED) of dusty galaxies typically peaks at 60-80 μm and can be approximated with a modified blackbody spectrum with dust temperatures between 30 and 80 K (Dunne et al. 2000). In host galaxies of quasi-stellar objects (QSOs), some dust can be directly heated by the central Active Galactic Nucleus (AGN) to higher temperatures; its emission then dominates the near- to mid-IR SED. For sources at high redshift ($z > 1$), the peak of the emission is shifted to submillimeter wavelengths, enabling useful multi-color photometric observations with ground-based telescopes in the submillimeter (submm) and millimeter (mm) atmospheric windows. Tracing the peak of their SED is crucial for an accurate determination of the IR luminosity and star formation rate in such dusty, energetic systems.

In principle, a determination of the SED peak could be expected to be useful for estimating the source redshift in cases where spectroscopic redshifts are not available. While this method has been shown to work in limited Monte Carlo simulations (Wiklind 2003; Hughes et al. 2002), there is the distinct possibility that it may be impractical, as the redshift and dust temperature are largely degenerate (Blain, Barnard, & Chapman 2003). Sampling the SED of high-redshift IR-luminous galaxies through the several submm and mm atmospheric windows (usually 350, 450, 850μm, 1.2, 2.0, 3.0 mm) has been achieved for only a few high-z sources (Benford et al. 1999; Priddey & McMahon 2001, and references therein).

Here we present observations at 350 μm of six quasars in the redshift range $1.8 \lesssim z \lesssim 6.4$. This doubles the number of high-z quasars for which such measurements are

available. The optically luminous and radio-quiet quasars were selected from the 1.2 mm continuum surveys performed with the Max-Planck Millimeter Bolometer (*MAMBO*) array by Omont et al. (2001, 2003) and Bertoldi et al. (2003a) - see Table 1. The selected wavelength of 350 μm roughly corresponds to the peak in the SEDs of highly redshifted emission from dust with temperatures of 40 to 60 K. We adopt the concordance Λ-cosmology with $H_0 = 71$ km s^{-1} Mpc^{-1}, $\Omega_\Lambda = 0.73$ and $\Omega_m = 0.27$ (Spergel et al. 2003).

2. Observations

The measurements were made on January 6 and 7, 2004 at the 10.4 m Leighton telescope of the Caltech Submillimeter Observatory (CSO) on the summit of Mauna Kea, Hawaii, during excellent weather conditions, with stable zenith atmospheric opacities of 1.0 at 350 μm. We used the CSO bolometer camera, SHARC II, described by Dowell et al. (2003), moounted at the reimaged Cassegrain focus. It consists of a 12×32 array of doped silicon 'pop-up' bolometers operating at 350 μm. Under good weather conditions, the point-source sensitivity at 350 μm is ~ 1 Jy/$\sqrt{\mathrm{Hz}}$ or better. The detectors of SHARC II cover the focal plane with 90% filling factor and are separated by $0.70\,\lambda/D = 4.86''$.

Pointing was checked regularly on strong sources including planets and secondary calibrators, and the focus was checked at the beginning of each night. The pointing was found to be stable with a typical accuracy of $\lesssim 2''$ (1σ r.m.s). We used the Dish Surface Optimization System (DSOS) which actively corrects the 10.4-meter primary surface for static imperfections and deformations due to gravitational forces as the dish moves in elevation (Leong et al. 2005). The DSOS improves the beam shape and provides an elevation-independent telescope efficiency $\sim 10\%$ better than the passive telescope (which has an aperture efficiency of 33% at 350 μm) at intermediate elevation and 50% better at high elevation. The beam of the CSO at 350 μm is approximated by a circular Gaussian

with a FWHM of $8\farcs5$. Uranus served as a primary flux calibrator and the asteroids Pallas and Ceres as secondary calibrators. At the time of the observations, the brightness temperature of Uranus was 64 K and its diameter $3\farcs4$, corresponding to a 350 μm flux density of 224 Jy. The secondary calibrators Pallas, Ceres and IRC10216 had 350 μm flux densities of 7.0, 40 and 24 Jy, respectively, as derived by various observation made with SHARC II using Mars, Uranus and Neptune as primary calibrators, with uncertainties of 15% based on repeatability of observations. The absolute calibration was found to be accurate to within 20% at 95% confidence.

SHARC II was also used at 450 μm to observe APM 08279+5255 on January 13, 16 and 18, 2004 under good weather conditions ($\tau_{225\ \mathrm{GHz}} \sim 0.09$). For these observations, we used as the secondary calibrators Ceres and IRC+10216 which had flux densities at 450 μm of 28 and 13 Jy, respectively.

The observations were performed by scanning the SHARC II array in azimuth and elevation using Lissajous and box-scan patterns with amplitudes of $15\farcs0 \times 14\farcs14$ and $25\farcs0 \times 35\farcs22$, respectively, in order to reduce systematic errors. The SHARC II array is rectangular, of $2\farcm61 \times 0\farcm96$ in extent, with the long axis oriented in azimuth. The sources were also observed at different elevations before and after transit. The final maps have typical sizes of $\approx 2 \times 1$ arcmin^2. At 350 μm, the total integration time per map is between 150 and 430 minutes, with the exception of APM 08276+5255, which was only observed for only 20 minutes. The corresponding rms map noise values are in the range from 5 to 15 mJy (Table 1).

The data were reduced using the 1.42 version of the software package *CRUSH* (Comprehensive Reduction Utility for SHARC II; Kovàcs 2006, in preparation). *CRUSH* is based on an algorithm that solves a series of models which try to reproduce the observations through an iterative process, taking into account instrumental and atmospheric

effects while using statistical estimators on the data. For the current data, we used the option *deep* which is appropriate for sources with typical flux densities smaller than 1 Jy/beam. To derive the flux densities of the high-z quasars at 350 and 450 μm, we fitted circular Gaussians profiles and a uniform background level, leaving the position, the full width half maximum and the intensities as free parameters. The resulting noise maps were used to derive the statistical uncertainties on the fitted parameters which served to estimate the uncertainty on the flux densities. These uncertainties do not take into account the calibration errors.

3. Results

All six quasars were detected at significance levels of $>\sim 3.5\,\sigma$ (Table 1). The signal maps of the 350 μm continuum emission are shown in Fig. 1. In the following, we comment on the individual sources.

KUV 08086+4037 This $z = 1.78$ broad emission line quasar was discovered by Darling & Wegner (1996) and detected at 1.2 mm by Omont et al. (2003). The mm to 1.4 GHz radio continuum flux ratio is compatible with a star-forming galaxy Petric et al. (2006, in preparation). We detect KUV 08086+4037 at 350 μm with a flux density of 69 ± 11 mJy. The peak emission of KUV 08086+4037 is shifted by 3 to $\sim 4''$ from the optical or radio position, corresponding to $\sim 2\sigma$ of the pointing accuracy of the CSO. However, it is unlikely that the detected emission does not come from the QSO, and the offset is probably due to a pointing model problem.

APM 08279+5255 This is a strongly lensed $z = 3.91$ broad absorption line quasar with a bolometric luminosity of $\sim 10^{14}$ $L_\odot$ after correction for magnification by a factor 7 (Downes et al. 1999). It is a strong IR/submm source which was even detected by IRAS

(Irwin et al. 1998). Its mid-IR spectrum was observed with the *Spitzer Space Telescope*, confirming a strong continuum likely due to the dust heated by the AGN (Soifer et al. 2004). The massive reservoir of dust (a few $\sim 10^8\,\mathrm{M}_\odot$) and warm molecular gas (3×10^9 $\mathrm{M}_\odot$) associated with this quasar is distributed in a nuclear disk of radius 100-200 pc around the Active Galactic Nucleus (AGN), and traces a dynamical mass of $1.5 \times 10^{10}\,\mathrm{M}_\odot$ (Lewis et al. 2002). With a 350 μm flux density of 386 ± 32 mJy, APM 8279+5255 is the strongest high-z source ever detected at 350 μm. The flux density at 450 μm measured with SHARC II is 342 ± 26 mJy, and were found to be stable over the three different observations periods, 319 ± 32 mJy on January the 13rd, 279 ± 111 mJy on the 16th and 418 ± 52 mJy on the 18th. This flux density is higher than the 211 ± 47 (68) mJy reported by Lewis et al. (1998) and the 285 ± 11 (40) mJy found by Barvainis & Ivison (2002), but is still compatible with them within 1σ, when taking into account the absolute calibration uncertainties of SCUBA, as quoted in parenthesis and estimated to be of the order of 10%.

HS 1002+4400 is a quasar at $z = 2.08$ which was first discovered in the Hamburg survey (Hagen et al. 1999). It displays broad emission lines with no peculiar features, and it was detected at 1.2 mm by Omont et al. (2003) and in the 1.4 GHz radio continuum by Petric et al. (2005). The radio to mm continuum flux ratio is consistent with that of a starburst. HS 1002+4400 is detected at 350 μm with a flux density of 77 ± 14 mJy.

SDSS J114816.64+5251, hereafter refered to as J1148+5251, is the most distant quasar ($z = 6.42$) known to date (Fan et al. 2003). An optically very luminous quasar, powered by a supermassive black hole, it also shows strong far-IR emission with an estimated luminosity of 1.2×10^{13} $\mathrm{L}_\odot$ (Bertoldi et al. 2003a), and an implied rate of star formation of ≈ 3000 $\mathrm{M}_\odot$ yr^{-1}. A massive reservoir of dense molecular gas ($\approx 2 \times 10^{10}$ $\mathrm{M}_\odot$) is implied by the observed CO emission (Walter et al. 2003; Bertoldi et al. 2003b) and the recent detection of the [CII] emission line (Maiolino et al. 2005). The 1.4 GHz radio

continuum flux follows the radio-FIR correlation for star-forming galaxies (Carilli et al. 2004). J1148+5251 as been detected both at 850 and 450μmby Robson et al. (2004), with flux densities of 7.8 ± 0.7 mJy and 24.7 ± 7.4 mJy respectively. Charmandaris et al. (2004) reported the detection of J1148+5251 with the *Spitzer Space Telescope* at 16 and 22 μm, revealing a hot dust component that could be heated by the AGN; however, it should be noted that these measurement are also compatible with the emission of the AGN extrapolated from the optical. We detected J1148+5251 at 350 μm with a flux density of 21 ± 6 mJy at the optical position of the QSO. This is the lowest flux density ever detected at 350 μm. A map with the best fit source subtracted present only noise, with any residual sources < 14 mJy, meaning that the apparent source extension seen in figure 1 is due to noise.

J140955.5+562827, hereafter refered to as J1409+5628, at $z = 2.56$ is an optically very bright, radio-quiet quasar. It is by far the strongest mm source in the Omont et al. (2003) MAMBO survey of $z \approx 2$ quasars. It has a massive reservoir of warm and dense molecular gas which is detected in CO (Beelen et al. 2004) and HCN (Carilli et al. 2005), with an estimated mass of 6×10^{10} M$_\odot$. Its far-IR luminosity of $\sim 4 \times 10^{13}$L$_\odot$ implies a star formation rate of several 1000 M$_\odot$ yr^{-1} (Beelen et al. 2004). The radio flux density is consistent with the radio-FIR correlation for star-forming galaxies Petric et al. (2006, in preparation). High resolution VLBA observations resolve out the radio emission, implying an intrinsic brightness temperature of $\sim 10^5$ K at 8 GHz, which is typical for nuclear starbursts (Beelen et al. 2004). The 350 μm flux density of 112 ± 12 mJy places J1409+5628 among the strongest submm high-z sources.

PSS 2322+1944 is an optically luminous, lensed (magnification $a = 3.5$) quasar at $z = 4.12$. It was detected in mm dust and radio continuum, and in various CO emission lines (Omont et al. 2001; Cox et al. 2002; Carilli et al. 2002). With a far-IR luminosity

of $9 \times 10^{12}\, L_{\odot}$ (corrected for lensing), it harbours a massive reservoir of molecular gas detected in CO, where star formation takes place with a rate of ≈ 1000 M$_{\odot}$ yr^{-1}. The CO line emission is resolved into an Einstein ring, which can be modeled as a disk of dense and warm molecular gas surrounding the QSO with a radius of $\sim 2\,$kpc, tracing a dynamical mass of a few 10^{10} M$_{\odot}$ (Carilli et al. 2003). PSS 2322+1944 is clearly detected at 350 μm with a flux density of 79 ± 11 mJy.

4. Discussion

The thermal emission from dust at a temperature $T_{\rm dust}$, is proportional to $B_\nu(T_{\rm dust})[1 - e^{-\tau_d}]$, where $B_\nu(T_{\rm dust})$ is the Planck function and $\tau_d(\lambda) = \kappa(\lambda) \int \rho\, ds$ is the dust optical depth, with κ being the mass absorption coefficient at rest wavelength λ and ρ the total mass density. At far-IR wavelengths $\lambda > 40$ μm, the emission is optically thin, $\tau_d \ll 1$, so that the above expression applied to a given dust mass at redshift z leads to an emergent flux density

$$\begin{aligned} S_{\nu_{\rm o}} &= \frac{(1+z)}{{D_{\rm L}}^2}\, M_{\rm dust}\, \kappa(\nu_{\rm r})\, B_{\nu_{\rm r}}(T_{\rm dust}) \qquad (1) \\ &\propto \nu_{\rm r}^{3+\beta}\, \frac{1}{\exp(h\nu_{\rm r}/kT_{\rm dust}) - 1}, \qquad (2) \end{aligned}$$

where the mass absorption coefficient, $\kappa(\nu) = \kappa_0 (\nu/\nu_0)^\beta$, is approximated by a power law.

Dusty galaxies typically show multi-temperature components in their IR SEDs. At rest frame near- and mid-IR wavelengths, the emission from these quasars arises from a "hot" (several 100 K) but not very massive dust component, that is likely heated directly by the AGN. The far-IR emission, on the other hand, arises from starburst regions where most of the energy emerges from dust with temperatures in the range 30 to 80 K, but by mass, most of the dust could be in a 10-20 K component that is energetically overpowered by the warmer component.

Through a fit of a single temperature greybody (3 free parameters: luminosity or integrated intensity, β and $T_{\rm dust}$), the dust temperature and emissivity index can be determined simultaneously only if *at least* 4 photometric data points are available (fit with more than one degree of freedom). For most objects, only two photometric data points (S_1 and S_2 at ν_1 and ν_2) are available, resulting in a degeneracy between the dust temperature and β (Priddey & McMahon 2001; Blain, Barnard, & Chapman 2003):

$$\alpha e^{h\nu_1/kT_{\rm dust}} - e^{h\nu_2/kT_{\rm dust}} = \alpha - 1, \tag{3}$$

where $\alpha = (\nu_2/\nu_1)^{3+\beta}\ S_1/S_2$.

4.1. Individuals objects

We fit a modified black (grey) body spectrum (Eq. 1) to the rest frame 40 to 800 μm SEDs of the six high-z quasars we observed at 350 μm. To account for the uncertainties in the absolute calibration of the submm and mm photometry, we added 20% to the uncertainties of all measurements.

For those quasars where only two photometric data points are available, we fixed $\beta = 1.6$ (see §. 4.2) and derived $T_{\rm dust}$ from Eq. 3. When more photometric measurements are available, we performed a χ^2-fit on $T_{\rm dust}$ only, or both $T_{\rm dust}$ and β when the degree of freedom in the fit was greater than one, except in the case of J1148+5251 were the lack of detection in the Rayleigh-Jeans domain prevent the fit of β. The resulting fits are shown in Fig. 2 for four of the quasars where three or more measurements are available. Figure 2 also shows the available radio, near- and mid-IR measurements, as well as the radio continuum emission expected from the correlation between the far-IR and radio luminosity observed in nearby star-forming galaxies (Condon 1992).

The far-IR luminosity is found by integrating over the fitted modified black body. The

mass $M_{\rm dust}$ of dust at $T_{\rm dust}$ is related to far-IR luminosity by

$$L_{\rm FIR} = 4\pi\ M_{\rm dust} \int \kappa(\nu) B_\nu(T_{\rm dust})\ d\nu, \tag{4}$$

or to the flux density $S_{\nu_{\rm obs}}$ observed at frequency $\nu_{\rm obs}$ (See Eq. 1)

A major source of uncertainty in estimating the dust mass comes from uncertainties of the mass absorption coefficient κ, which is poorly constrained by observations or laboratory experiments. We adopt a value of 0.4 cm^2/g at 1200 μm, which is in the range of values found in the literature (Alton et al. 2004, and references therein). For each source, the derived temperature, spectral index, luminosity, and dust mass are listed in Table 2.

The dust spectral index could be fitted for only two of our sources, APM 08279+5255 and PSS 2322+1944, resulting in $\beta = 1.9 \pm 0.3$ and 1.5 ± 0.3, respectively. The fixed value of $\beta = 1.6$ for the other sources is based on the mean SED discussed in § 4.2. Our values are consistent with those found for dusty local galaxies: $1.3 \leq \beta \leq 2.0$ (Dunne et al. 2000; Priddey & McMahon 2001; Alton et al. 2004, and references therein), and are slightly lower than the $\beta = 2$ expected for pure silicate and/or graphite grains (Draine & Lee 1984).

The derived temperatures for the warm dust are in the range 30 to 60 K, which is typical for local IR-luminous galaxies, where the heating is dominated by young massive stars (Dunne et al. 2000). The values are also comparable to those found for other high-z sources (Benford et al. 1999). Our single-component fits do not account for the hot dust component that dominates at rest frame mid-IR wavelengths. For APM 08279+5255, e.g., when adopting $\beta = 1.9$, a two dust component fit to the SED between 10 and 800 μm yields $T_{\rm hot} = 155 \pm 17$ K and $T_{\rm warm} = 45 \pm 2$ K. The warm dust temperature well agrees with the value found from a single dust component fit. The situation is similar for the Cloverleaf, where a single component fit yields $T_{\rm dust} = 38 \pm 3$ K and $\beta = 2.0 \pm 0.2$, whereas a two-component fit with fixed $\beta = 2$ yields $T_{\rm hot} = 118 \pm 13$ K and $T_{\rm warm} = 36 \pm 1$ K, which also agrees with the results of Weiß et al. (2003). The same applies in the case of

IRAS F10214+4724 with a single component fit yields to $T_{\rm dust} = 44 \pm 7\,{\rm K}$ with β fixed to 1.6, and a two component fit to $T_{\rm hot} = 93 \pm 12$ K and $T_{\rm warm} = 41 \pm 8\,{\rm K}$. These three examples (see fig 3) suggest that the temperatures found for the warm dust from single component fits are not much affected by the hot dust component – although this probably depends somewhat on the relative intensities of both components. Further measurements at the rest frame peak emission, from 10 to 100 μm, are needed to clearly solve this problem, note that a dust temperature distribution is more likely to be found, instead of a single or two dust components.

The derived dust masses range from a few 10^8 to 10^9 $M_\odot$ (Table 2), indicating huge reservoirs of gas in the high-z quasars. However, uncertainties in these mass estimates arise from the assumed value of the mass absorption coefficient κ, which is constrained only within a factor of 4 (Alton et al. 2004). Furthermore, there may well be a cold dust component which emission would remain hidden below that of the warm component even if it contained up to three times the mass of the warm component (Dunne et al. 2000; Dunne & Eales 2001).

4.2. Dust temperature and spectral index of the mean far-IR SED of high-z quasars

The determination of both β and $T_{\rm dust}$ is currently possible only for a few objects. Even when enough photometric data points are available for individual sources, the uncertainties on the temperature and the spectral index are large and the $\beta - T_{\rm dust}$ degeneracy prevents reliable estimates of the far-IR luminosities.

To better constrain the mean properties of the high-redshift quasar warm dust component, we have fitted a single temperature grey body to the photometric points of all

quasars with at least two measurements in the rest frame far-IR. This provides a useful empirical description of the mean far-IR SED of dusty high-z galaxies, which can be used as a template to derive the far-IR luminosities when only a few photometric measurements are available. The 14 quasars of this sample have redshifts in the range 1.8 to 6.4, which provides a "wavelength coverage" of the ensemble SED much wider than that possible for individual objects. Figure 4 shows the resulting mean SED.

A similar analysis was done by Priddey & McMahon (2001) for a smaller sample of $z > 4$ quasars, where they found $T_{\rm dust} = 41 \pm 5$ K and $\beta = 1.95 \pm 0.3$. Instead of iteratively normalizing the SEDs, we left the normalization of each SED a free parameter in the combined fit. Thereby no prior assumption is made on the scale, but each source SED needs two or more far-IR flux measurements to bring at least one degree of freedom to the fit. The best fit values, $T_{\rm dust} = 47 \pm 3$ K, $\beta = 1.6 \pm 0.1$, the χ^2 contours and the $\beta - T_{\rm dust}$ degeneracy are shown in Fig. 5. The fitted SED is overplotted on the ensemble of scaled measurements in Fig. 4. Although consistent (within 1σ) with the results of Priddey & McMahon (2001), our findings suggest a somewhat higher dust mean temperature and lower β.

The derived mean spectral index of $\beta = 1.6 \pm 0.1$ is not consistent with the value of $\beta = 2$ expected for dust grains made of pure silicates and/or graphites (Draine & Lee 1984). However, a range of dust temperatures will lower the effective measured β. For example, the sum of two modified black-bodies with dust temperatures $T_{\rm warm}$, $T_{\rm cold}$ and $\beta = 2$ provides a fit to the mean far-IR SED that is as good as the one with a single dust temperature and $\beta = 1.5$ - see also Dunne & Eales (2001). The mean value of $\beta = 1.6$ was adopted in § 4.1 to fit the dust temperature for sources with only a few photometric measurements. The current data does not well constrain an additional cold component, for which measurements at longer wavelengths, 2 to 3 mm, would be most valuable.

4.3. Infrared to Radio spectral index

For local star-forming galaxies a tight linear correlation is found between the radio continuum (monochromatic) luminosity, $L_{1.4\,\mathrm{GHz}}$, and the far-IR luminosity, L_{FIR}, with a scatter of a factor $\approx 2-3$ over more than four orders of magnitude in luminosity (Condon 1992; Yun, Reddy, & Condon 2001). This tight relation is generally understood to be due to star-formation activity, measuring the dust heated by young stars, and the radio synchrotron emission from supernova remnants. That this relation also holds at higher redshifts was shown by Appleton et al. (2004), who report evidence for its validity out to $z = 2$ by matching *Spitzer Space Telescope* 24 and 70 μm sources and VLA radio sources. In the following, we check whether the Condon correlation also holds for high-z far-IR-luminous quasars.

The far-IR/radio relationship is usually quantified by a parameter

$$q \equiv \log(\frac{L_{\mathrm{FIR}}}{3.75\times10^{12}\,\mathrm{W}}) - \log(\frac{L_{1.4\,\mathrm{GHz}}}{\mathrm{W\,Hz^{-1}}}), \tag{5}$$

where $L_{1.4\,\mathrm{GHz}}$ is the monochromatic rest frame 1.4 GHz luminosity (Helou, Soifer, & Rowan-Robinson 1985; Condon 1992), L_{FIR} is the far-IR luminosity, which was originally computed from the rest frame 60 and 100 μm IRAS fluxes (Helou, Soifer, & Rowan-Robinson 1985) under the assumption of a typical dust temperature of $\approx 30\,\mathrm{K}$. However, these definitions are not practical for ULIRGs that have higher dust temperatures, and we therefore use the integrated far-IR luminosity of the warm dust component.

To compute the radio luminosities we fitted a power-law to the observed radio flux densities and extrapolate to the rest frame 1.4 GHz flux density. When only one data point is available, we use a radio spectral index of -0.75 (Condon 1992).

The resulting q values are listed in Table 2. Figure 6 plots the radio luminosity against the far-IR luminosity for the 2 Jy galaxy sample of Yun, Reddy, & Condon (2001). To be

consistent with our definitions, we recomputed the far-IR luminosities by fitting a single dust temperature modified black-body with $\beta = 1.6$. The figure compares the Yun sample to the high-z quasars sample, except for HS 1002+4400 where no radio data are available (see the caption of Fig 6 for details).

Most of our quasars well follow the far-IR/radio correlation well, showing a median $q = 2.2 \pm 0.4$, in good agreement with the value of 2.3 ± 0.1 found for the Yun sample. Two quasars show unusually high radio to far-IR flux ratios: BRI $0952 - 0115$ which shows a radio luminosity similar to that of a low-luminosity radio galaxy (Yun et al. 2000) and the Cloverleaf, which contains a known weakly radio-loud AGN.

The fact that the high-z quasars reasonably follow the Condon relation for star-forming galaxies suggests that their radio and far-IR emission do also arise from star formation, although a weak contribution from the AGN is not excluded. Further evidence for this is provided by the vast amounts of dense molecular gas detected in CO line emission for some of the quasars (see § 3) , and by the implied several kpc spatial extent of these gas reservoirs, which is very similar to that of the starbursts rings resolved in nearby Seyfert and starburst galaxies (García-Burillo et al. 2003).

5. Conclusions

This paper reports sensitive measurements of 350 μm dust emission from high-redshift quasars. The detection of six $1.8 \leq z \leq 6.4$ quasars doubles the number of quasars at high redshift for which 350 μm photometry is available. Combined with observations at mm/submm wavelengths, the 350 μm data allow us to sample the rest frame far-IR SEDs of these high-z sources and, thereby, to constrain the properties of their warm dust emission. The 350 μm measurements are key in deriving the far-IR luminosities since they sample the

peak of the warm dust emission. For the high-z quasars, the derived temperatures are in the range 40 to 60 K and the luminosities are a few $10^{13}\,L_{\odot}$. The derived dust masses range from a few 10^{8} to $10^{9}\,M_{\odot}$.

The mean far-IR SED of all high-z quasars measured with two or more rest frame far-IR data points is best fit with a grey-body of temperature, $T_{\rm dust} = 47 \pm 3\,{\rm K}$ and a dust emissivity spectral index, $\beta = 1.6 \pm 0.1$. However, note that there are considerable variations and uncertainties in the determination of the dust temperature and spectral index in individual objects, which is not reflected in the quoted uncertainties here. To determine accurately β and T_{dust}, a good sampling of the SED, especially along the Rayleigh-Jeans part of the modified blackbody is needed with measurements around the emission peak. Photometric measurements at high-frequency (e.g., at 350 μm) are important to sample the peak of the redshifted far-IR emission and derive the far-IR luminosity, whereas data at low frequencies (2 or 3 mm) would be key to constrain β. Future facilities such as the Atacama Large Millimeter Array (ALMA) will improve the sensitivity in the submm/mm regime by more than an order of magnitude relative to current instrumentation and will enable the measurement of the SEDs of high-z sources over a wide range in frequency with a precise calibration, including much less luminous and extreme objects than the ones which can be observed today.

All the radio-quiet high-z quasars studied in this paper approximately follow the far-IR/radio correlation, showing a median $q = 2.2 \pm 0.4$, consistent with that found for local star-forming galaxies. This result is a further indication that, in these high-z radio-quiet quasars, the radio and far-IR emission does arise from star formation.

The warm (40-60 K) dust component found from single component fits to the SEDs of high redshift quasars is not much affected by the presence of a hot (several 100 K) dust component that dominates at rest frame mid-IR wavelengths, as shown by the examples

of APM 08279+5255 and the Cloverleaf. The warm dust component is thus found to be a relatively good tracer of the starburst activity of the quasars's host galaxy. More mid-IR measurements are needed to assess the degree to which the warm and hot dust components can be treated independently in high-z quasars. In this respect, the *Spitzer Space Telescope* will provide valuable photometric data at mid-IR wavelengths and allow us to build complete SEDs for a number of high redshift quasars from their rest frame near- to far-IR wavelengths to investigate the relative importance of the AGN and starburst activity.

The CSO is funded by the NSF under contract AST02-29008. A.B. acknowledges financial support from the Programme National de Galaxies. We thank A. Jones and F. Boulanger for fruitful discussions on the subject of this work.

REFERENCES

Alton, P. B., Xilouris, E. M., Misiriotis, A., Dasyra, K. M., & Dumke, M. 2004, A&A, 425, 109

Appleton, P.N., Fadda, D.T., Marleau, F.R. et al. 2004, ApJS, 154, 147

Barvainis, R. & Ivison, R. 2002, ApJ, 571, 712

Beelen, A., Cox, P., Pety, J. et al. 2004, A&A, 423, 441

Benford, D.J., Cox, P., Omont, A., Phillips, T.G., & R.G. McMahon 1999, ApJ, 518, L65

Bertoldi, F., Carilli, C.L., Cox, P. et al. 2003a, A&A, 406, L55

Bertoldi, F., Cox, P., Neri, R., et al. 2003b, A&A, 409, L47

Blain, A.W., Barnard, V.E., & Chapman, S.C. 2003, MNRAS, 338, 773

Carilli, C. L., et al. 2001, ApJ, 555, 625

Carilli, C.L., Cox, P, Bertoldi, F. et al. 2002, ApJ, 575, 145

Carilli, C.L., Lewis, G.F., Djorgovski, S.G. et al. 2003, Science, 300, 773

Carilli, C. L., et al. 2004, AJ, 128, 997

Carilli, C. L., et al. 2005, ApJ, 618, 586

Charmandaris, V., et al. 2004, ApJS, 154, 142

Condon, J. J. 1992, ARA&A, 30, 575

Cox, P., Omont, A., Djorgovski, S.G. et al. 2002, A&A, 387, 406

Darling, G. W. & Wegner, G. 1996, AJ, 111, 865

Dowell, C. D., Allen, C.A., Babu, R. et al. 2003, Proc. SPIE, 4855, 73

Downes, D., Neri, R., Wiklind, T., Wilner, D. J., & Shaver, P. A. 1999, ApJ, 513, L1

Dunne, L., Eales, S., Edmunds, M., Ivison, R., Alexander, P., & Clements, D. L. 2000, MNRAS, 315, 115

Dunne, L. & Eales, S. A. 2001, MNRAS, 327, 697

Draine, B. T. & Lee, H. M. 1984, ApJ, 285, 89

Fan, X., et al. 2003, AJ, 125, 1649

García-Burillo, S., Combes, F., Hunt, L.K. et al. 2003, A&A, 407, 485

Greve, T. R., Bertoldi, F., Smail, Ian, et al. 2005, MNRAS, 359, 1165

Hagen, H.-J., Engels, D., & Reimers, D. 1999, A&AS, 134, 483

Helou, G., Soifer, B. T., & Rowan-Robinson, M. 1985, ApJ, 298, L7

Hughes, D. H., Aretxaga, I., Chapin, E. L. et al. 2002, MNRAS, 335, 871

Irwin, M. J., Ibata, R. A., Lewis, G. F., & Totten, E. J. 1998, ApJ, 505, 529

Leong M. M. 2005, URSI Conf. Sec. J3-10, 426, http://astro.uchicago.edu/ursi-comm-J/ursi2005/rf-telescope-fabrication/leong

Lewis, G. F., Chapman, S. C., Ibata, R. A., Irwin, M. J., & Totten, E. J. 1998, ApJ, 505, L1

Lewis, G. F., Carilli, C., Papadopoulos, P., & Ivison, R. J. 2002, MNRAS, 330, L15

Maiolino, R., et al. 2005, A&A, 440, L51

Omont, A., Cox, P., Bertoldi, F. et al. 2001, A&A, 374, 371

Omont, A., Beelen, A., Bertoldi, F. et al. 2003, A&A, 398, 657

Petric, A., Carilli, C.L., Bertoldi, F. et al. 2004, AJ, submitted

Priddey, R.S., & McMahon, R.G. 2001, MNRAS, 324, L17

Robson, I., Priddey, R.S., Isaak, K. & McMahon, R.G. 2004, MNRAS, 351, L29

Spergel, D. N., et al. 2003, ApJS, 148, 175

Soifer, B. T., et al. 2004, ApJS, 154, 151

Walter, F., Bertoldi, F., Carilli, C.L. et al. 2003, Nature, 424, 406

Weiß, A., Henkel, C., Downes, D., & Walter, F. 2003, A&A, 409, L41

Wiklind, T. 2003, ApJ, 588, 736

Yun, M. S., Carilli, C. L., Kawabe, R., Tutui, Y., Kohno, K., & Ohta, K. 2000, ApJ, 528, 171

Yun, M. S., Reddy, N. A., & Condon, J. J. 2001, ApJ, 554, 803

This manuscript was prepared with the AAS LaTeX macros v5.2.

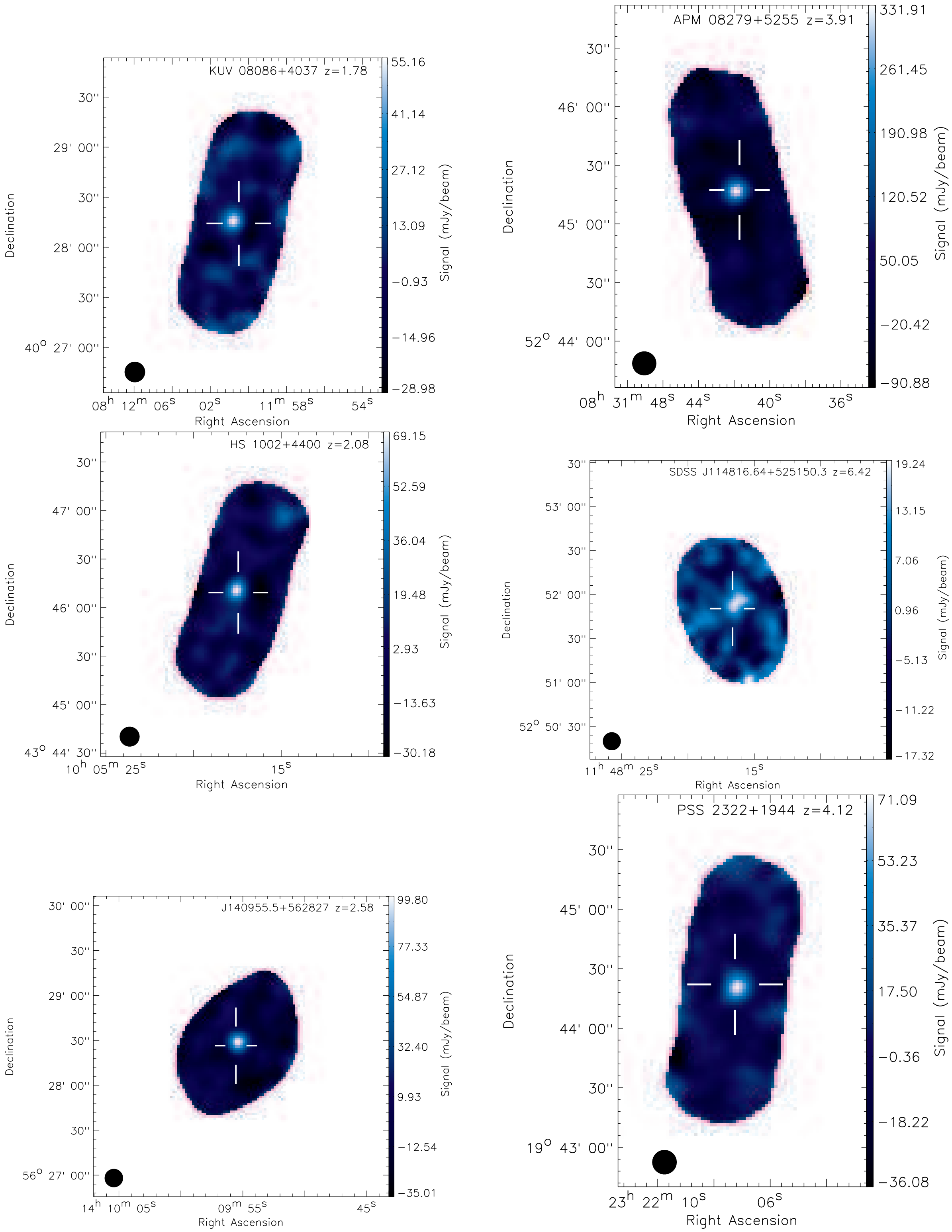

Fig. 1.— SHARC II maps at 350 μm of the six optically luminous, radio-quiet high-z quasars studied in this paper. The names and redshifts are given in the upper left corner of each panel. The maps have been cut to half of the maximum exposure, and smoothed with a 9″ FWHM Gaussian.The resulting beam size is shown in the lower left corner of each plot.

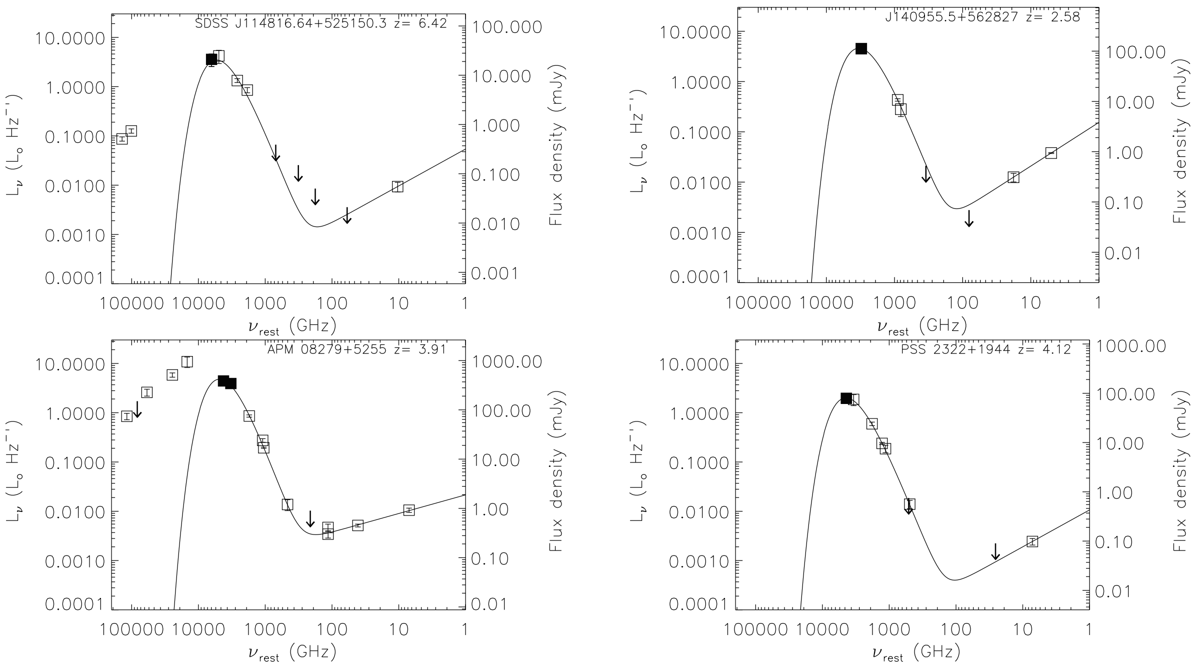

Fig. 2.— Spectral energy distributions (SEDs) of J1148+5251, J1409+5628, APM 08279+5255 and PSS 2322+1944 in the rest frame of the sources. The SHARC II 350 and 450 μm points are shown as filled squares. Other measurements (taken from the literature) are displayed with open squares with arrows indicating 3σ upper limits. The solid line shows the best fit to the far-IR data using a modified black-body and to the radio using a power-law (see text and parameters in Table 2). When needed the radio spectral index was set to 0.75. The references to the photometric measurements other than from SHARC II are: J1148+5251 - Bertoldi et al. (2003a); Carilli et al. (2003, 2004); Robson et al. (2004); Charmandaris et al. (2004); J1409+5628 - Omont et al. (2003); Beelen et al. (2004); Petric et al. (2005); PSS 2322+1944 Cox et al. (2002, and references therein); APM08279+5255 - Irwin et al. (1998); Lewis et al. (1998, 2002); Downes et al. (1999).

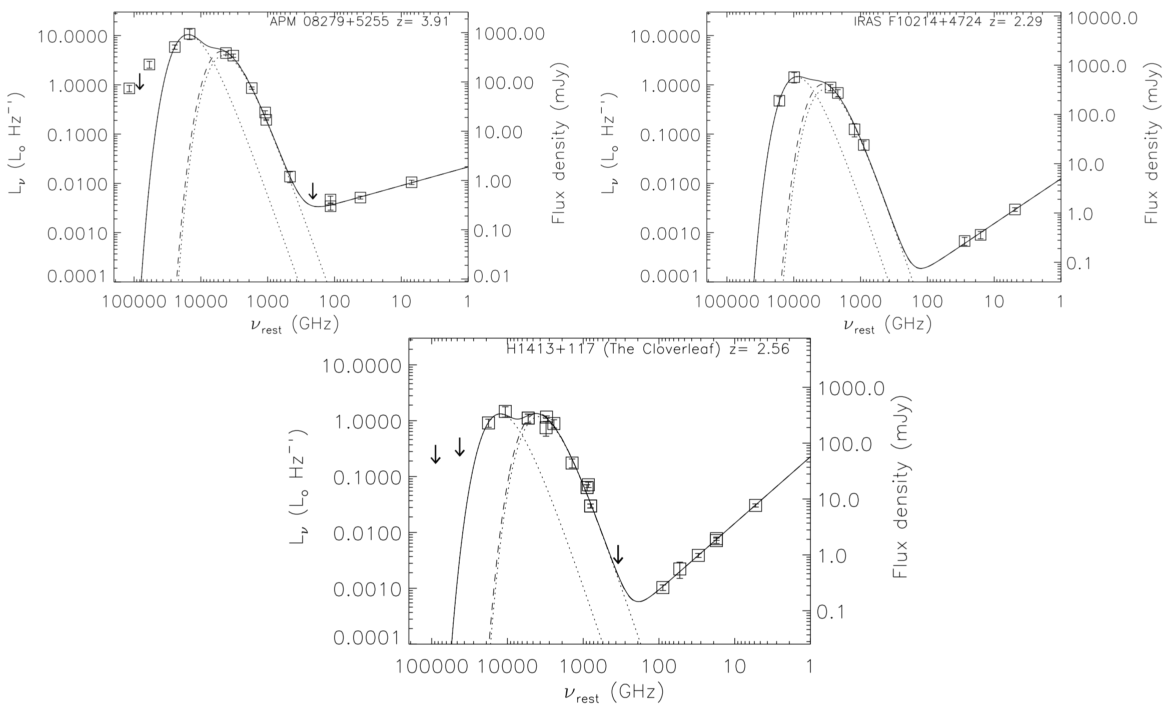

Fig. 3.— SEDs of APM 08279+5255, IRAS 10214+4724 and the Cloverleaf in the rest frame of the sources. The solid line shows the best fit to the mid/far-IR data using two components model (plain and dotted line) and to the radio using a power-law (see text for parameters). The dashed line correspond to a single component fit to the far-IR data.

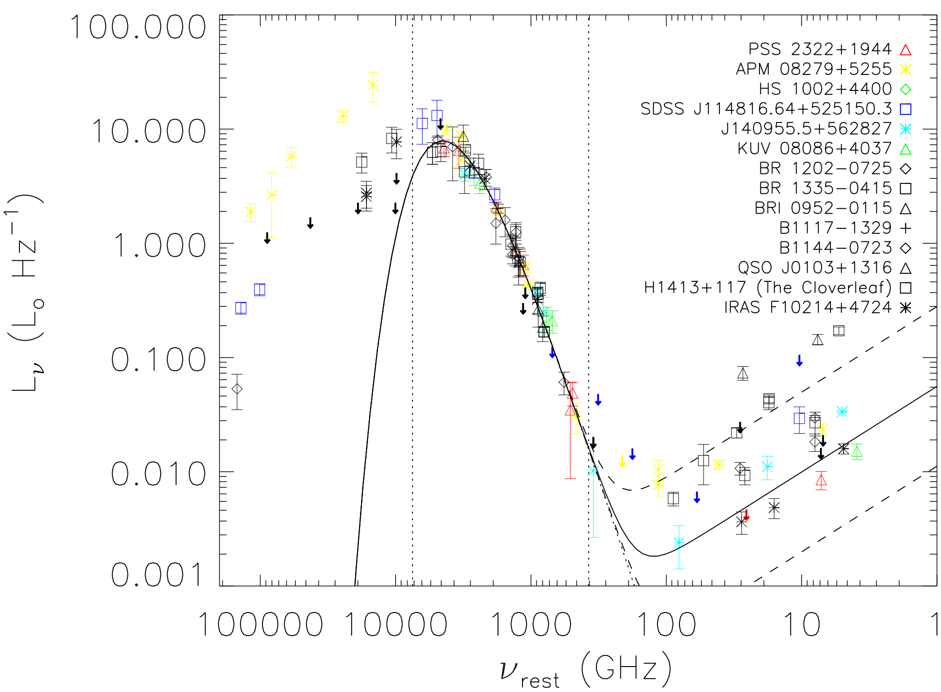

Fig. 4.— Combined SED, in the rest frame, for all the high-z quasars from this paper and sources discussed in Benford et al. (1999) and Priddey & McMahon (2001) (see references therein and in Fig. 2). The SEDs have been normalized to the far-IR luminosity of PSS 2322+1944. Each quasar is represented with a different symbol identified in the panel. The best fit to the rest frame far-IR data together with the derived radio continuum are shown using the same definitions as in Fig. 2. The corresponding dust temperature and spectral index are displayed in Fig. 5. The two vertical dot-dashed lines delineate the wavelength domain defined as the far-IR in this paper.

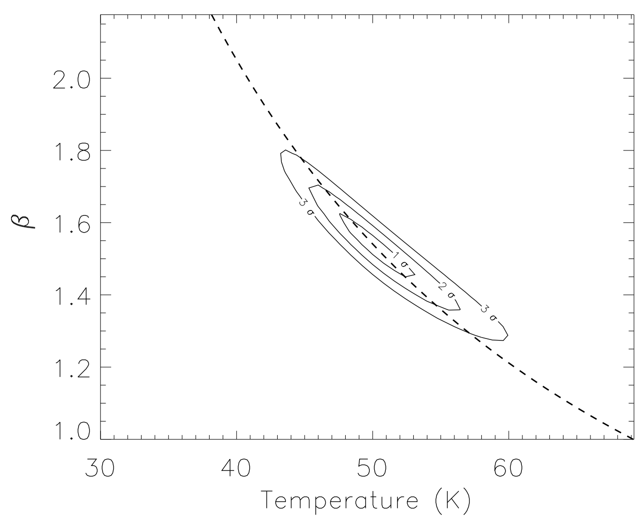

Fig. 5.— Contours of χ^2 in the $\beta - T_{\rm dust}$ plane for the combined SEDs of the high-z quasars shown in Fig. 4. Contours represent the 1, 2, and 3σ uncertainties. The dashed line represents the $\beta - T_{\rm dust}$ degeneracy (see text for details).

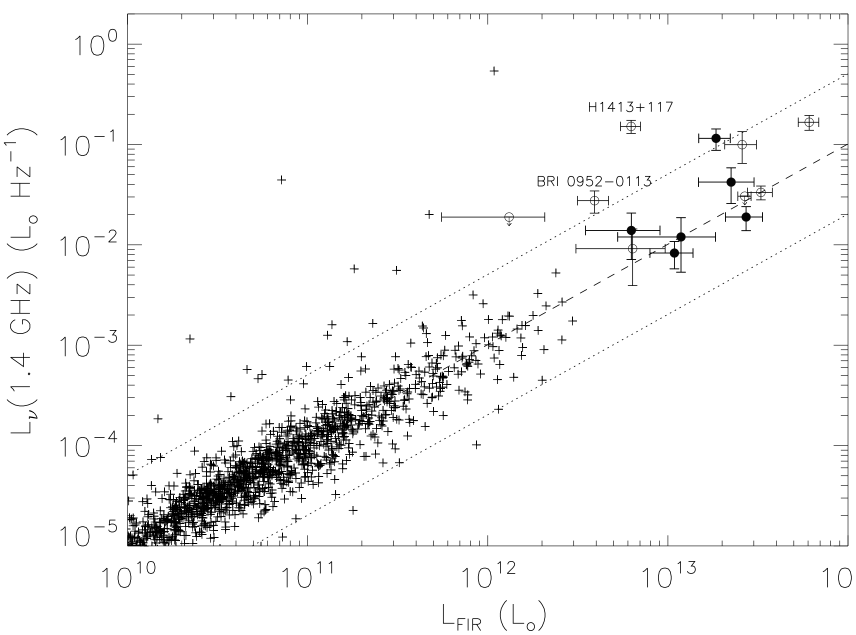

Fig. 6.— rest frame 1.4 GHz luminosity as a function of the $L_{\rm FIR}$ as defined by Condon (1992) - see text. The crosses are for the IRAS 2 Jy sample of Yun, Reddy, & Condon (2001) and the circles for the sources discussed in this paper which have radio detection (filled circles are sources from Table 1, whereas open circles are sources taken from the literature and listed in Fig. 4). The dashed line shows the mean value of q while the dotted lines display the IR and radio excesses which are 5 times above and below the value expected from the linear far-IR/radio relation. When known, the luminosities of the high-z sources have been corrected for lensing.

Table 1: Observational Parameters.

Source	z	$M_{\rm B}$	R.A.	Dec.	$S_{1.2\rm mm}$	$S_{350\mu\rm m}$	Int. time
			(J2000.0)		(mJy, $\pm 1\sigma$)	(mJy, $\pm 1\sigma^{\dagger}$)	(min)
KUV 08086+4037	1.78	−27.0	08 12 00.41	40 28 15.00	$4.3 \pm 0.8^{\rm a}$	69 ± 11	180
APM 08279+5255‡	3.91	−32.9	08 31 41.70	52 45 17.35	$24 \pm \ \ 2^{\rm b}$	386 ± 32	20
HS 1002+4400	2.08	−28.3	10 05 17.45	43 46 09.30	$4.2 \pm 0.8^{\rm a}$	77 ± 14	170
J1148+5251	6.42	−28.4	11 48 16.64	52 51 50.30	$5.0 \pm 0.6^{\rm c}$	$21 \pm \ \ 6^{+}$	430
J1409+5628	2.58	−28.4	14 09 55.56	56 28 26.50	$10.7 \pm 0.6^{\rm a}$	112 ± 12	220
PSS 2322+1944	4.12	−28.1	23 22 07.25	19 44 22.08	$9.6 \pm 0.5^{\rm d}$	79 ± 11	150

† The absolute calibration uncertainty of 20% is not included in the quoted values

‡ For APM 08279+5255, the flux density measured at 450 μm with SHARC II is 342 ± 26 mJy

+ The flux density for J1148+5251 is derived with a FWHM of 11.″5.

[a] Omont et al. (2003)

[b] Irwin et al. (1998) at 1.35 mm

[c] Bertoldi et al. (2003a)

[d] Omont et al. (2001)

Table 2: Derived Properties.

Source	T_{dust} (K)	β	amp. factor	L_{FIR} (10^{13} $L_\odot$)	Dust Mass (10^8 $M_\odot$)	q
KUV 08086+4037	32 ± 5	1.6^+	–	0.6 ± 0.3	23.8	2.1 ± 0.2
APM 08279+5255	47 ± 7	1.9 ± 0.3	7[1]	2.7 ± 0.7	5.7	2.6 ± 0.1†
HS 1002+4400	38 ± 7	1.6^+	–	1.2 ± 0.7	17.3	
J1148+5251	55 ± 5	1.6^+	–	2.2 ± 0.7	4.5	2.2 ± 0.2
J1409+5628	35 ± 2	1.6^+	–	1.8 ± 0.4	48.8	1.4 ± 0.2‡
PSS 2322+1944	47 ± 8	1.5 ± 0.3	3.5[2]	1.1 ± 0.3	6.8	2.5 ± 0.1

The far-IR luminosities and dust masses are corrected for lensing amplification when indicated.

The references to the amplification factor are : [1] Lewis et al. (2002), [2] Carilli et al. (2003).

$^+$ fixed value

† $\alpha_{\rm radio} = -0.35 \pm 0.07$

‡ $\alpha_{\rm radio} = -1.0 \pm 0.1$